Australas Phys Eng Sci Med (2017) 40:85–99
DOI 10.1007/s13246-016-0512-4

SCIENTIFIC PAPER

An automated microemboli detection and classification system using backscatter RF signals and differential evolution

Karim Ferroudji[1] · Nabil Benoudjit[1] · Ayache Bouakaz[2]

Received: 7 April 2016 / Accepted: 28 November 2016 / Published online: 9 January 2017

Abstract Embolic phenomena, whether air or particulate emboli, can induce immediate damages like heart attack or ischemic stroke. Embolus composition (gaseous or particulate matter) is vital in predicting clinically significant complications. Embolus detection using Doppler methods have shown their limits to differentiate solid and gaseous embolus. Radio-frequency (RF) ultrasound signals backscattered by the emboli contain additional information on the embolus in comparison to the traditionally used Doppler signals. Gaseous bubbles show a nonlinear behavior under specific conditions of the ultrasound excitation wave, this nonlinear behavior is exploited to differentiate solid from gaseous microemboli. In order to verify the usefulness of RF ultrasound signal processing in the detection and classification of microemboli, an in vitro set-up is developed. Sonovue micro bubbles are exploited to mimic the acoustic behavior of gaseous emboli. They are injected at two different concentrations (0.025 and 0.05 µl/ml) in a nonrecirculating flow phantom containing a tube of 0.8 mm in diameter. The tissue mimicking material surrounding the tube is chosen to imitate the acoustic behavior of solid emboli. Both gaseous and solid emboli are imaged using an Anthares ultrasound scanner with a probe emitting at a transmit frequency of 1.82 MHz and at two mechanical indices (MI) 0.2 and 0.6. We propose in this experimental study to exploit discrete wavelet transform and a dimensionality reduction algorithm based on differential evolution technique in the analysis and the characterization of the backscattered RF ultrasound signals from the emboli. Several features are evaluated from the detail coefficients. It should be noted that the features used in this study are the same used in the paper by Aydin et al. These all features are used as inputs to the classification models without using feature selection method. Then we perform feature selection using differential evolution algorithm with support vector machines classifier. The experimental results show clearly that our proposed method achieves better average classification rates compared to the results obtained in a previous study using also the same backscatter RF signals.

Keywords Microemboli · Gaseous embolus · Solid embolus · Radio frequency signals · Ultrasound · Differential evolution

Introduction

Embolism is intravascular migration of an insoluble body such as gas bubble, a fat globule, a blood clot, an atheromatous plaque, or a piece of thrombus. Embolus formation inside the body could be attributed due to different physiological, physical, and intervention mechanisms [1]. It can travel to any part of the body, accounting for many serious (and sometimes life-threatening) disorders thus the importance of an automatic classification system.

Transcranial Doppler (TCD) [1] is a non-invasive ultrasound approach employed to assess blood flow velocity in the major basal intracranial arteries on a real time basis. In order to evaluate the ability of TCD to detect and classify intracranial emboli, several experimental studies have been carried since the early 1960s. One of the approaches relies on detecting the appearance of abrupt changes (known as

✉ Karim Ferroudji
karim_hab@hotmail.com

[1] Laboratoire d'Automatique Avancée et d'Analyse des Systèmes (LAAAS), Université de Batna-2, Fesdis, Algeria

[2] UMR Inserm U930-Imagerie et cerveau, Université François Rabelais de Tours, Tours, France

high intensity transient signals) in the TCD waveform with higher amplitudes than the other recorded signal. These abrupt changes are exploited as indicators of the presence of emboli, in several clinical areas: carotid and cardiac surgery [2, 3], cerebral angiography and following prosthetic heart valve insertion [4–6]. Many reports emphasized the ability of TCD, combined with signal processing methods for example discrete wavelet transform (DWT), to detect microemboli in the brain circulation [7–10]. Aydin et al. [7]. used a signal-processing algorithm based on DWT to characterize embolic signals (ES), Doppler speckle, or artifacts. In their work, they showed that the detection parameters derived from DWT coefficients are likely to improve the sensitivity of an automated system [7]. Unfortunately, this technology presents today some limitations to determine the embolus composition [11, 12]. Especially, before performing interventional procedures for neuroprotection where the nature of the emboli is a vital diagnostic criteria. This is the case during cardiac surgery and carotid endarterectomy where solid and gaseous embolus are strongly intricate. TCD can detect a high intensity transient signals indicating a presence of emboli but it is very difficult to differentiate gaseous from solid microemboli. Solid emboli involve different therapeutic approaches than gaseous emboli [13] and they are potentially far more damaging.

Indeed, when solid emboli are identified, an antiagregant or anticoagulant treatment will be employed. However, gaseous emboli are considered as a risk indicator and their detection involves to investigate for the cause of emboli.

Recently, a new approach based on the analysis of backscatter radio frequency signals using the nonlinear characteristics of gaseous bubbles and artificial neural network to classify emboli was investigated [13, 14]. A number of researchers have reported that DWT performs better than fast Fourier transform (FFT) for the analysis and the detection of ES [7, 15]. The existence of fast algorithms to implement DWT, makes also the investigation of the feasibility of ES detection systems based on the DWT worthwhile.

We suggest in this experimental study to exploit Radio-Frequency ultrasound signals backscattered by the emboli since they contain additional information on the embolus in comparison to the classically used Doppler signals [16].

First, we employ DWT algorithm based on the Daubechies (db6) to decompose RF signals into different frequency bands and identify which features lead to a better recognition performance. Several features are evaluated from the detail coefficients. It should be noted that the features used in this study are the same used in the work by Aydin et al. [7]. These features are used as inputs to the classification models without using feature selection method. Second, and due to curse of dimensionality, we employ a wrapper feature selection approach based on differential evolution (DE) algorithm. This algorithm, referred to as differential evolution feature selection (DEFS).

Feature selection techniques usually fall into three main categories; filter, wrapper, or embedded methods. Filter approaches perform feature selection using the intrinsic properties of the data independently of the learning algorithm. Wrapper approaches conduct feature selection using a learning algorithm as part of the evaluation function to estimate the relevance of a given set of features, in embedded approaches the search for an optimal set of features is built into the learning algorithm construction [17].

DEFS utilizes the differential evolution float number optimizer in a combinatorial optimization problem like feature selection. The DEFS highly reduces the computational cost while at the same time proves to present a powerful performance [18, 19].

In order to evaluate the performance of the proposed system, we implemented SVM classifier. For nonlinear classification problem with limited number of samples SVMs appear to be advantageous compared to neural networks approaches [20–22]. Furthermore, in [23] a detailed comparison of SVM, radial basis neural network, and K-nearest neighbor is performed. The results indicated that SVM approach demonstrated superior performance compared to the other two classifiers, it was concluded that SVM has less sensitivity to the curse of dimensionality [23]. We use hold-out-set cross-validation strategy to fix the parameters of the classifier and to select the most relevant features. While there are other validation techniques, including, but not limited to, bootstrap and leave-one-out, we focus on the more commonly used cross-validation approach in this paper. We randomly divide the dataset, into two subsets training set and test set (hold-out-set). After that, we apply cross-validation technique only on the training set to randomly generate new training and validation sets. The test set is used only for the assessment of the model selected by the cross-validation algorithm. While the validation set is used to tune the parameters of the classifier. The experimental evaluation is performed using hold-out-set to avoid overfitting and assure statistical validity of the results [24].

The main purpose of this experimental study is to evaluate the performances of the proposed technique in the detection and classification of microemboli using Radio-Frequency ultrasound signals backscattered by the emboli instead of Doppler signals.

Discrete wavelet transform of backscatter RF signals

Discrete wavelet transform

The basic idea of the wavelet transform is to represent any arbitrary signal $x(t)$ as a superposition of a set of wavelets

or basis functions. These basis functions are obtained from a single prototype wavelet called the mother wavelet by dilation (scaling) and translation (shifts). The wavelet transform of a continuous signal *x(t)* is defined as [7, 25]:

$$c(a,b) = \int_R x(t)\frac{1}{\sqrt{a}}\psi\frac{(t-b)}{a}dt, \quad (1)$$

where, the indexes *c(a,b)* are called wavelet coefficients of signal *x(t)*, *a* is dilation and *b* is translation, $\Psi(t)$ is the mother wavelet. DWT of a signal is defined with respect to a mother wavelet and maps continuous finite energy signals to a two-dimensional grid of coefficients [7, 25]. The scale *a* in the discrete wavelet transform case becomes $a = a_0^m$, and the translation *b* becomes $b = nb_0a_0^m$ [7, 25]. DWT of a discrete signal with length *N* is defined as:

$$c(m,n) = \frac{1}{\sqrt{a_0^m}}\sum_{k=0}^{N-1} s(k)\,\psi\left(\frac{k - nb_0a_0^m}{a_0^m}\right). \quad (2)$$

DWT of a discrete signal yields a set of coefficients including all the detailed coefficients and the last approximation coefficients [7, 25].

DWT description of backscatter RF signals

The backscatter RF signal are transformed into different time–frequency scales through the wavelet analysis, DWT uses two functions as high-pass filters and low pass filters. The high-frequency filter generates a detailed version of the backscatter RF signal (*D*), while the low-frequency filter produces its approximate version (*A*).

In our study, we decomposed the backscatter RF signal *x(t)* into five levels, so we can write as:

$$x(t) = A5(t) + D5(t) + D4(t) + D3(t) + D2(t) + D1(t). \quad (3)$$

Wavelet functions used for this study are standard DWT functions available in Matlab Wavelet toolbox [26], namely Daubechies (db6). An example of the decomposition of gaseous embolus and solid embolus signals is shown in Fig. 1. The detail and approximation coefficients are not directly used as classifier inputs. In this study, several features are used. All features are individually applied to the detail coefficients of each decomposition level.

Detection algorithm

The general block diagram of the detection system is shown in Fig. 2. The input backscatter RF signals are first detected and collected (signal acquisition). At the second stage, DWT coefficients of the signals are collected. Input signals

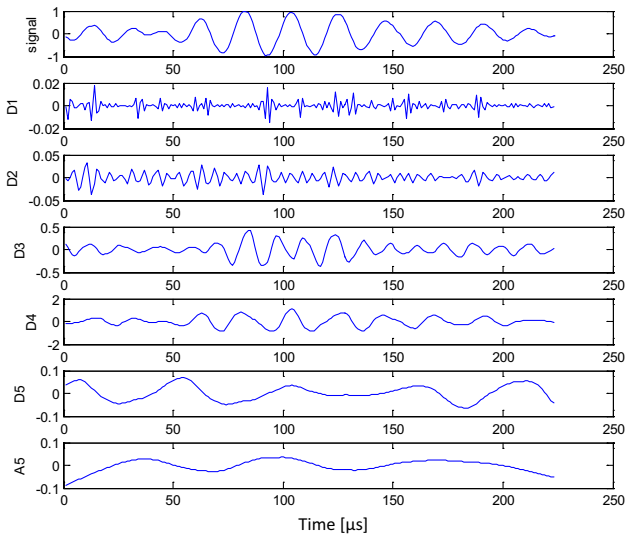

(a) Gaseous embolus

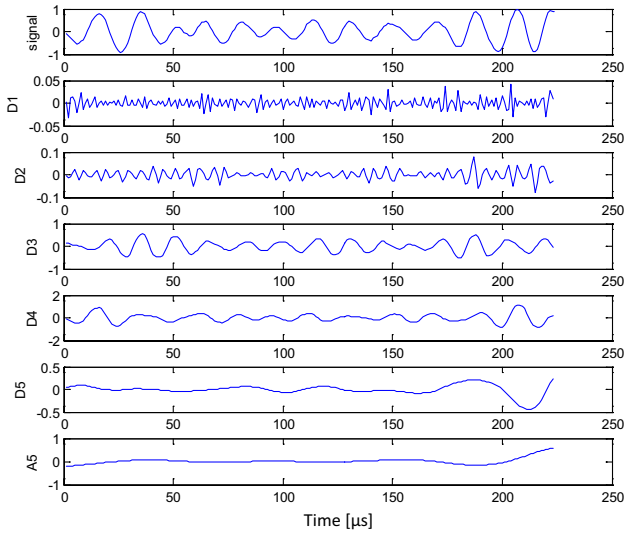

(b) Solid embolus

Fig. 1 Examples of DWT using Daubechies (db6) as mother wavelet of backscatter RF signal at low mechanical index (MI = 0.2)

are decomposed into an optimum number of frequency bands using DWT. Therefore, it is vital to select an appropriate wavelet for the signal being analyzed. Suitability of the wavelet filters and orders are determined experimentally. It should be noted that we shown in previous work that the best mother wavelet on the same types of backscatter RF signals is Daubechies (db6) [27]. In the third step, after applying DTW on the backscatter RF signals, several features are evaluated from the detail coefficients. It should be noted that the features used in this study are the same in the paper by Aydin et al. [7]. Table 2 shows the ten (10) features for each decomposition level and their formulas. In the last step, all these features are first used as inputs to the classification model without feature selection method.

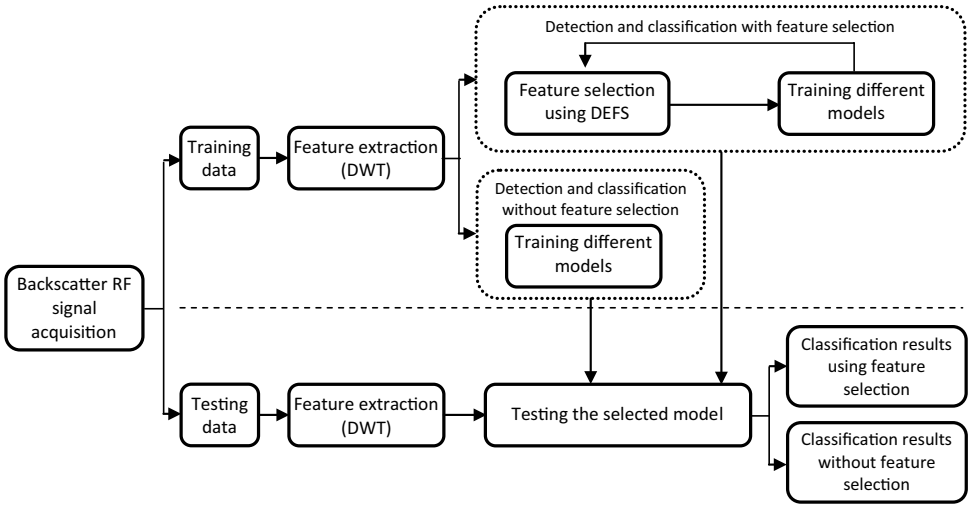

Fig. 2 Block diagram of the DWT-based detection system

Table 1 Confusion matrix for binary classification model

	Predicted	
	Gaseous emboli	Solid emboli
Actual class		
Gaseous emboli	TP	FP
Solid emboli	FN	TN

Where true positive (TP): the classifier predicts a label as gaseous emboli and the actual class is gaseous emboli, true negative (TN): the classifier predicts a label as solid emboli and the actual class is solid emboli, false positive (FP) the classifier predicts a label as solid emboli and the actual class is gaseous emboli, false negative (FN): the classifier predicts a label as gaseous emboli and the actual class is solid emboli

Second, due to the curse of dimensionality, we employ a feature selection algorithm based on DE algorithm [18, 19]. The motivation for this approach is that the more powerful among the existing machine learning algorithms tend to get confused when supplied with a large number of features [28].

Table 1 shows the confusion matrix in which the correct and incorrect predictions made by the classifier compared with the true labels in the test data are depicted.

Before classification and feature selection tasks, and since the generalization performance of an algorithm should be estimated using unseen samples, we randomly divided the dataset into two subsets (training set and test set). After that, we applied cross-validation technique only on the training set to tune the classifier parameters and to rank the features. Thus the algorithms have only access to the training set, and the test set is kept unseen both to the ranking step and to the classifying step. The experimental evaluation is performed using hold-out-set cross-validation to avoid overfitting and assure statistical validity of the results [24].

The reported results are obtained with different types of measures, such as classification accuracy, sensitivity, and specificity.

Accuracy: (Number of correct predicted labels)/(Number of all labels)

$$Accuracy = \frac{TP + TN}{TP + TN + FP + FN} \tag{4}$$

Sensitivity: proportion of actual positives which are predicted positive it can be expressed as:

$$Sensitivity = \frac{TP}{TP + FN} \tag{5}$$

and then Specificity which is the proportion of actual negative which are predicted negative:

$$Specificity = \frac{TN}{TN + FP} \tag{6}$$

Feature extraction

The instantaneous power (IP) is calculated for the DWT coefficients of each level. A threshold value for each level is determined. Figure 3 illustrates the associated IP and threshold values, which are used in the detection algorithm.

The threshold is calculated from the data using a statistical method, which depends on the data length and the standard deviation [29], and it is given by:

$$A_{\text{th}} = \sigma_{\text{n}} \sqrt{\log_2 N} \tag{7}$$

where: σ_{n} is the standard deviation of the signal power at the n^{th} level and N is the length of the observation.

The following parameters relating the threshold are determined:

The ratio of the embolic signal to the background signal (EBR) is the most widely used feature in microemboli detection [7]. EBR shows how strong an embolic signal is relative

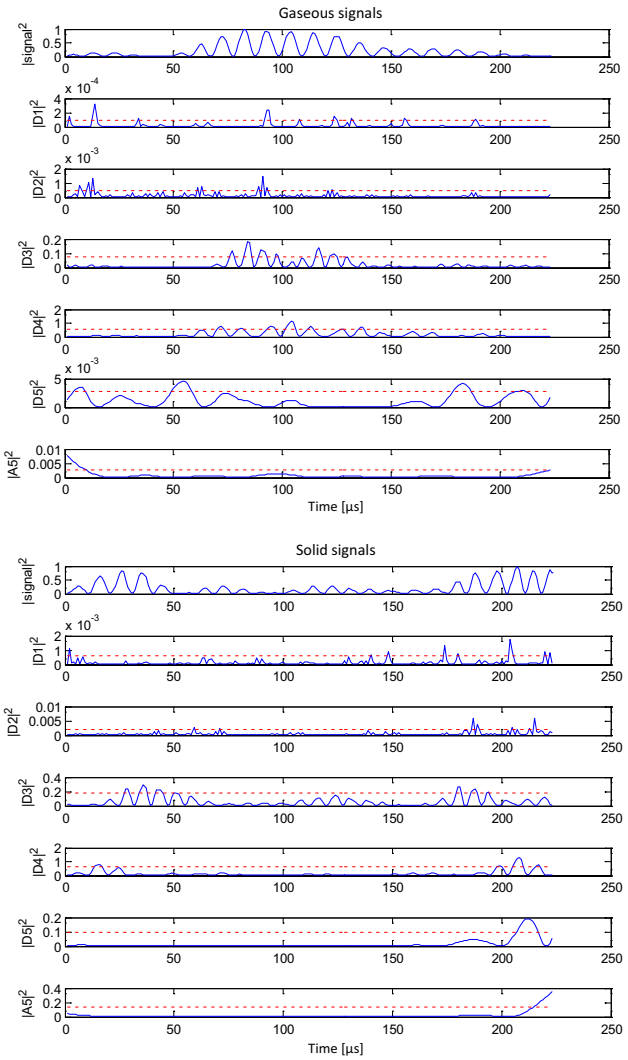

Fig. 3 Instantaneous power and corresponding threshold values for each level (gaseous and solid embolus signals)

to the background. *P2TR* is one of the definitions of the EBR, *P2TR* can be calculated using the measures given in Fig. 4.

$$\mathrm{P2TR} = 10 \log \frac{\mathrm{A_{pk}}}{\mathrm{A_{th}}} \ (\mathrm{dB}) \tag{8}$$

Another feature, the total power to the threshold ratio (TP2TR) which is the quantity of power a signal has relative to the background energy, and it is given by:

$$\mathrm{TP2TR} = 10 \ \log \frac{\mathrm{A_{tot}}}{\mathrm{A_{th}}} = 10 \ \log \frac{\sum_{k=t_{on}}^{t_{off}} \mathrm{A}_f(k)}{\mathrm{A_{th}}} \ (\mathrm{dB}) \tag{9}$$

where A_{tot} is the total power of the signal $A(k)$. It is calculated by integrating the *IP* of signal between t_{on} and t_{off}, as illustrated in Fig. 4.

Two other features, which use threshold indirectly, are rise rate (RR) and fall rate (FR):

$$\mathrm{RR} = \frac{10 \log \frac{\mathrm{A}_{pk}}{\mathrm{A_{th}}}}{\mathrm{t_{pk}} - t_{on}} = \frac{\mathrm{P2TR}}{\mathrm{t_{pk}} - t_{on}} \ (\mathrm{dB/ms}) \tag{10}$$

$$\mathrm{FR} = \frac{10 \log \frac{\mathrm{A}_{pk}}{\mathrm{A_{th}}}}{\mathrm{t_{off}} - t_{pk}} = \frac{\mathrm{P2TR}}{\mathrm{t_{off}} - t_{pk}} \ (\mathrm{dB/ms}) \tag{11}$$

where: t_s is the average time of the signal and f_s is the average frequency of the signal.

t_s and f_s are calculated, respectively, as

$$t_s = \frac{1}{E_s} \int_{-\infty}^{+\infty} t \mid s(t) \mid^2 dt \tag{12}$$

$$f_s = \frac{1}{E_s} \int_{-\infty}^{+\infty} f \mid S(f) \mid^2 df \tag{13}$$

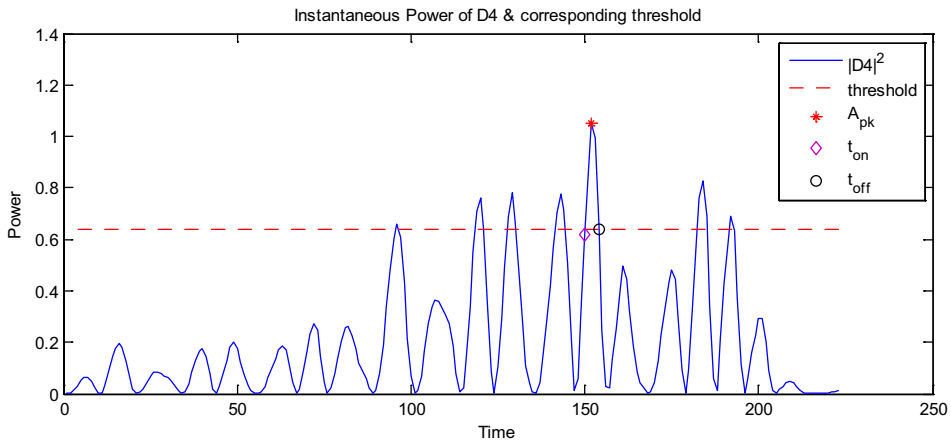

Fig. 4 Instantaneous power of the detail coefficient and parameters used to calculate detection features

where $S(f)$ is the Fourier transform of the signal $s(t)$.

Time spreading Ts^2 and frequency spreading Bs^2 are defined as:

$$T_s^2 = \frac{1}{E_s}\int_{-\infty}^{+\infty} (t - t_s)^2 |s(t)|^2 dt \tag{14}$$

$$B_s^2 = \frac{1}{E_s}\int_{-\infty}^{+\infty} (f - f_s)^2 |S(f)|^2 df \tag{15}$$

where:

$$E_s = \int_{-\infty}^{+\infty} |s(t)|^2 dt \tag{16}$$

The instantaneous envelope and instantaneous frequency of a signal [30] are used to describe a signal simultaneously in time and in frequency. These two parameters are defined, respectively, as:

$$a(t) = |s_a(t)| \tag{17}$$

$$f(t) = \frac{1}{2\pi}\frac{d(arg(s_a(t)))}{dt} \tag{18}$$

where $s_a(t)$ is the Hilbert transform of $s(t)$.

$$s_a(t) = s(t) + j\hat{s}(t).\hat{s}(t) \tag{19}$$

The variances of instantaneous envelope and instantaneous frequency (*VIE* and *VIF*) are used as other types of features.

Processing steps for the classification of microemboli can be summarized as follows:

- Apply DWT to both solid and gaseous signals in order to collect DWT coefficients;
- calculate Instantaneous power for each level;
- from each level, derive a threshold value to be employed in detection;
- evaluate previously described parameters for each DWT level;
- apply: (i) classification, (ii) dimensionality reduction.

Table 2 summarizes the feature extractor methods that are used in this study.

As shown in Fig. 3, and unlike all the detail coefficients, the approximation coefficients does not have a similar shape (peak or Gaussian) thus we can't extract the parameters t_{on} and t_{off}, therefore we discarded the approximation coefficients from the feature extraction phase.

Classification

For binary classification problems with limited number of samples it is crucial to validate the classification model

Table 2 The features used in this study for each decomposition level and their formulas

	Feature number (n)	Formulations of detail coefficients
$P2TR_n$	$n=1,\ldots,5$	$P2TR = 10\log\frac{A_{pk}}{A_{th}}(dB)$
$TP2TR_n$	$n=6,\ldots,10$	$TP2TR = 10\log\frac{A_{tot}}{A_{th}} = 10\log\frac{\sum_{k=t_{on}}^{t_{off}} A_f(k)}{A_{th}}(dB)$
RR_n	$n=11,\ldots,15$	$RR = \frac{10\log\frac{A_{pk}}{A_{th}}}{t_{pk}-t_{on}} = \frac{P2TR}{t_{pk}-t_{on}}(dB/ms)$
FR_n	$n=16,\ldots,20$	$FR = \frac{10\log\frac{A_{pk}}{A_{th}}}{t_{off}-t_{pk}} = \frac{P2TR}{t_{off}-t_{pk}}(dB/ms)$
t_{sn}	$n=21,\ldots,25$	$t_s = \frac{1}{E_s}\int_{-\infty}^{+\infty} t \mid s(t) \mid^2 dt$
f_{sn}	$n=26,\ldots,30$	$f_s = \frac{1}{E_s}\int_{-\infty}^{+\infty} f \mid S(f) \mid^2 df$
T_{sn}^2	$n=31,\ldots,35$	$T_s^2 = \frac{1}{E_s}\int_{-\infty}^{+\infty} (t-t_s)^2 \mid s(t)\mid^2 dt$
B_{sn}^2	$n=36,\ldots,40$	$B_s^2 = \frac{1}{E_s}\int_{-\infty}^{+\infty} (f-f_s)^2 \mid S(f)\mid^2 df$
VIE_n	$n=41,\ldots,45$	$var(a(t))$ with $a(t) = \mid s_a(t) \mid$ where $s_a(t) = s(t) + j\hat{s}(t).\hat{s}(t)$, $\hat{s}(t)$ is the Hilbert transform of $s(t)$
VIF_n	$n=46,\ldots,50$	$var(f(t))$ with $f(t) = \frac{1}{2\pi}\frac{d \arg s_a(t)}{dt}$

where n is the number of the detail coefficient which is used to calculate the classification parameters

with cross validation technique. Before building the classification model, the samples are subdivided into three subsets training set, validation set, and test set. The test set is used only for the assessment of the model selected by the cross-validation technique, while the validation set is used to tune the classifiers parameter. Therefore the algorithm has only access to the training and validation sets, the test set is kept unseen in the selection process of the best model.

Our experimental data consists of 102 samples (51 solid embolus and 51 gaseous embolus). In order to evaluate the predictive ability of a model, we randomly divide the dataset, into three subsets training set, validation set, and test set. The test set, approximately one-third (1/3) of the data (14 solid embolus and 14 gaseous embolus), is used only for the assessment of the model selected by the cross-validation technique, while the rest of the data will belong to the learning set (used for building the models) which will be divided into a training set (approximately two-third) and a validation set (approximately one-third). The validation set is used to tune the classifiers parameter.

In order to evaluate the performance of the proposed system, we employ support vector machines classifier.

Support vector machines classifier

Support Vector Machines, proposed by Vapnik's group in 1995 [31], are supervised learning techniques based on a statistical learning theory. SVM has gained increasing interest in areas that range from regression estimation to pattern recognition, due to its great learning performance. Indeed, SVMs don't have local extrema problems that are present for traditional neural networks, which involve large numbers of training patterns [32].

SVM was originally designed for linear binary classification problems. For nonlinear classification, a transformation maps the data from the input space into a higher dimensional feature space that allows linear separation. We then seek the optimization separation plane in feature space using a kernel function. In our case, radial basis kernel is used to differentiate between solid embolus and gaseous. More details about recent developments of SVM can be found in [31–33].

The kernel parameter γ and the penalty parameter C are the two major parameters of the RBF applied in SVM-RBF which have to be set appropriately in order to improve SVM learning. γ is the width of RBF kernel. C is the regularization parameter of error which allows one to trade off training error versus model complexity. In order to empirically select the best classification model, the value of each parameter is varied in a given predefined range according to a grid search [34]. We carried out experiments by trying exponentially growing sequences of C and γ on the training set [34]. The combination that results in a model with highest validation accuracy is picked as the best choice of the classification problem and then used to accurately predict the testing set.

Feature selection based on differential evolution algorithm

The feature vector cited in "Discrete wavelet transform of backscatter RF signals" section is too large to be handled properly by a classifier during training. To overcome this curse of dimensionality, we apply a supervised feature selection approach based on DE algorithm which belongs to the family of evolutionary algorithms. Later DE has been successfully applied to a large number of problems for example feature selection [18, 19]. To solve an optimization problem, DE starts by iteratively modifying a randomly generated initial population of candidate solutions using a floating-point encoding instead of binary numbers [18, 19, 35]. This process is then enhanced using selection, mutation, and crossover operations. DE combines different randomly chosen populations ($X_{r0}, X_{r1},$ and X_{r2}) to create a mutant element ($V_{i,g}$) from the current generation g [19]:

$$V_{i,g} = X_{\mathrm{r0},g} + \mathrm{F} * \left(X_{r1,g} - X_{r2,g}\right) \tag{20}$$

where $\mathrm{F} \in (0,\ 1)$ is a scale factor that controls the rate at which the population evolves. The index g indicates the generation to which a vector belongs.

In addition, DE also uses discrete recombination (crossover), in order to construct trial vectors out of parameter values that have been copied from two different populations:

$$\mathrm{U}_{j,i,g} = \begin{cases} \mathrm{V}_{j,i,g} & \text{if rand } (0\ ,\ 1) \le C_r \text{ or} \\ \mathrm{X}_{j,i,g} & \text{otherwise,} \end{cases} \tag{21}$$

where $\mathrm{U}_{j,i,g}$is the j'th trial element along i'th dimension from the current population g and $\mathrm{C}_r \in [0,\ 1]$ is the crossover probability which controls the fraction of parameter values that are copied from the mutant.

If the newly generated element results in a better fitness (classification accuracy) than the predetermined population member, then the resulting element replaces the vector with which it was compared.

The steps used in DEFS algorithm are [18, 19]:

- Generate new population elements from the original population.
- Create a new mutant vector for each position in the population matrix.
- A trail vector is obtained by crossing the mutant vector with the original vector.
- The corresponding position in the new population will contain either:

  - the trial vector or its corrected version,
  - or the original target vector depending on which one of them achieved a better fitness.

- The process is repeated until each of the population elements have competed against a randomly generated trial element.

Once the last trial element has been evaluated, the survivors of the population pairwise competitions become parents for the next generation in the evolutionary cycle. For further details on the above DEFS method, please refer to [18, 19].

Datasets

In order to verify the usefulness of RF ultrasound signal processing for microemboli classification, an in vitro setup is developed. It consists of a Doppler flow phantom containing 3 tubes of 0.2, 0.4 and 0.8 mm in diameter. The tube of 0.8 mm is chosen since its size approximates the size of a human vessel (Fig. 5). In order to imitate the ultrasonic behavior of gaseous emboli, contrast agents consisting of microbubbles are used in our experimental setup. Indeed, several studies have revealed that the acoustic behavior of gaseous emboli and microbubbles are similar, mainly the nonlinear behavior [14, 36]. Hence, a continuous flow carries the Sonovue microbubbles [37, 38] (contrast microbubbles) through the insonified vessel is used to mimic the ultrasonic behavior (scattering) of gaseous emboli. We used Sonovue microbubbles since it is the only commercially available contrast agent in Europe. The concentration of microbubbles and the flow are controlled by the operator. Since in clinical situations the scattering amplitude of emboli approaches that of blood, we fixed the concentration of Sonovue microbubbles such as its scattering amplitude at the fundamental frequency is comparable to the scattering of the surrounding tissue at the same frequency.

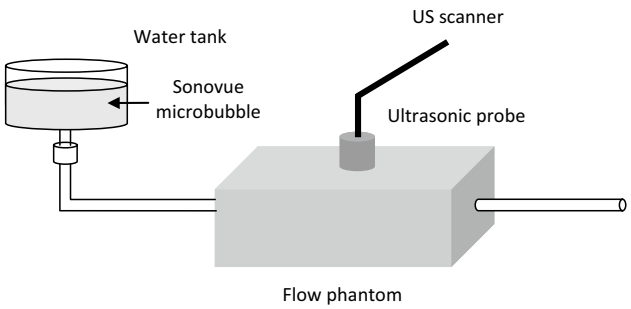

Fig. 5 Experimental set-up

However, solid emboli present acoustic properties comparable to those of biological tissue, in their scattered signal no harmonic components can be seen, therefore the scattering of solid emboli is purely linear. Thus the tissue mimicking material surrounding the vessel is chosen to mimic the behavior of solid emboli. Moreover, the applied acoustic pressures are not sufficiently high to induce nonlinear propagation effects and does not generate any harmonic components during ultrasound propagation.

The ultrasound waves are generated by a VF13-5 probe connected to a Siemens Antares scanner (Anthares, Siemens, MV, CA). The acquisitions are carried out at 1.82 MHz transmit frequency in Tissue Harmonic Imaging (THI) mode at 14 fps frame rate, and 20 MHz as the sampling rate of the signals. The acoustic focus is set at 2 cm which is the depth at which the flowing contrast microbubbles are situated. Ultrasound waves are transmitted at two different intensities corresponding to mechanical indices (MI) of 0.2 (low MI) and 0.6 (high MI). The User Research Interface is used to grab the unfiltered RF signals to a personal computer for further analysis. Two concentrations of contrast agent/Isoton were used: 0.025 and 0.05 µl/ml [13].

The regions of interests where RF signals corresponding to gaseous embolus and solid embolus are shown in Fig. 6.

Figure 7 illustrates two types of RF signals extracted from the obtained grayscale images. Panel a shows RF signal backscattered by gaseous and solid embolus at low MI (0.2). It is noteworthy that the acoustic pressure is not enough to create nonlinear microbubbles oscillations. Panel b illustrates the RF signal of each type of embolus

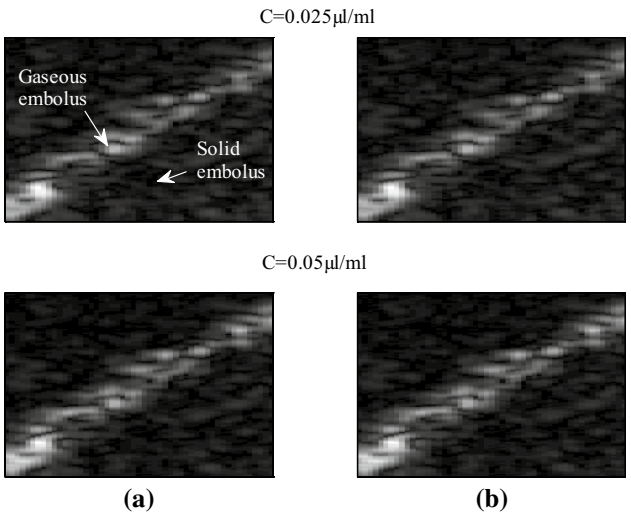

Fig. 6 Grey scale images acquired: **a** MI = 0.2, **b** MI = 0.6 for two microbubbles concentrations

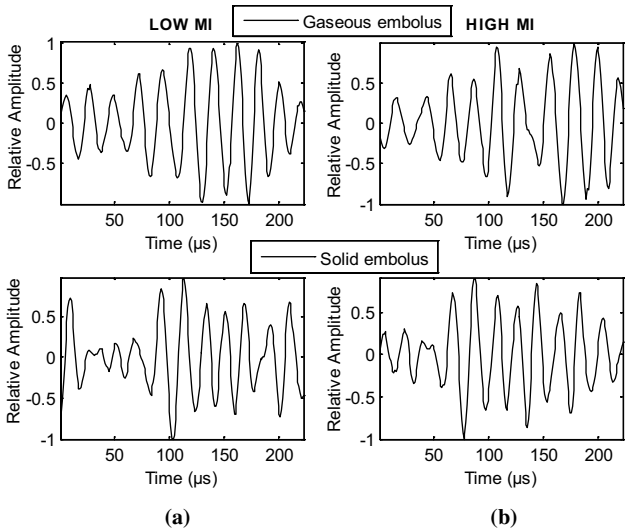

Fig. 7 Examples of RF signals. **a** MI = 0.2, **b** MI = 0.6

at higher MI (0.6) in this case the propagation of an ultrasound wave becomes nonlinear, thus a nonlinear behavior of both gaseous and solid particles is observed [13].

Results

Classification performance is evaluated in terms of two measures, which are: (i) the overall accuracy, which is the percentage of correctly classified embolus among all the embolus independently of the classes they belong to; (ii) the accuracy of each class that is the percentage of correctly classified embolus among the embolus of the considered class.

Table 3 summarizes the percentage of correct classification rates of microemboli using SVM analysis as a function of all input features (50 features) and mechanical indexes for the two microbubble concentrations (0.025 and 0.05 μl/ml).

The average classification rate doesn't exceed 85.71% for all datasets using all features as input vector. Therefore the feature vector is too large to be handled properly by the classifier. To overcome this limitation, we grouped the input parameters into small feature vectors regarding the nature of each feature then we applied the classification algorithm on each set of features separately, the results are shown in Table 4.

The features $P2TR_n$, RR_n, FR_n, and VIF_n for the two concentrations do not provide significant classification

Table 3 Classification rates of gaseous and solid emboli using all features

Average rate (%)	C = 0.025 μl/ml		C = 0.05 μl/ml	
	Low MI (0.2)	High MI (0.6)	Low MI (0.2)	High MI (0.6)
Sensitivity (gaseous emboli)	92.86	78.57	85.71	92.86
Specificity (solid emboli)	78.57	85.71	85.71	78.57
Accuracy	85.71	82.14	85.71	85.71

Table 4 Classification rates of gaseous and solid emboli using each set of features separately

Accuracy (%)	C = 0.025 μl/ml		C = 0.05 μl/ml	
	Average rate		Average rate	
Features	Low MI (0.2)	High MI (0.6)	Low MI (0.2)	High MI (0.6)
$P2TR_n$	71.42	60.71	82.14	82.14
$TP2TR_n$	85.71	85.71	85.71	82.14
RR_n	75.00	71.42	75.00	85.71
FR_n	82.14	75.00	78.57	71.42
t_{sn}	**89.28**	89.28	**89.28**	82.14
f_{sn}	**89.28**	89.28	85.71	82.14
T^2_{sn}	85.71	85.71	**89.28**	**89.28**
B^2_{sn}	85.71	85.71	85.71	**89.28**
VIE_n	**89.28**	**92.85**	**89.28**	82.14
VIF_n	64.28	75.00	75.00	64.28

The best results appear in bold

rates neither at low MI (0.2) nor at high MI (0.6). When the features TP2TR$_n$, t_{sn},f_{sn}, T^2_{sn}, B^2_{sn}, and VIE_n are introduced as input parameters into the SVM model, the correct average rate of classification of microemboli reached 89.28%, thus a significant improvement in the classification rates is observed.

In order to reduce the dimensionality we perform feature selection using differential evolution algorithm. DEFS algorithm is a wrapper approach; it performs feature selection using SVM classifier. We select the set of features that maximizes accuracy of the classification model (refer to Fig. 8).

Figure 8 draws the evolution of the average classification rate vs number of selected features at low microbubble concentration (0.025 µl/ml) with a higher MI (0.6), the best result (Accuracy = 96.42%) is obtained using four features. The training data set is used to select the most relevant features and to fix the parameters of the classifier. The final results presented, are based on the system's performance using one unseen test data set.

The output of the designed approach using DEFS algorithm and SVM classifier based on hold-out-set cross validation are illustrated in Table 5.

For the concentration of microbubbles (0.025 µl/ml) at low MI (0.2) our proposed method achieved 96.42% classification rate using a total of 4 features. For the other three acquisitions the performance measures are quite similar, the proposed method reached a classification rate of 92.85%.

More particular parameters can also be derived, such as the sensitivity and the specificity of the classification system (refer to Eqs. 5, 6) which are used to discriminate relevant information that provide more insight into the characteristics of the model in order to make meaningful decisions. Sensitivity relates to a test's ability to correctly identify those patients with pathology as positive. Specificity of a test refers to its ability to correctly identify individuals without the pathology as negative. Furthermore, we investigated other statistical measure which better estimates the accuracy of a given trial test by analyzing sensitivity and specificity simultaneously, this approach is the area under curve (AUC) associated to the receiver operating characteristic (ROC) curve. AUC allows to quantify the ROC curve performance using a single value. It is well known that the higher the AUC value, the more efficient the classifier.

Figure 9 shows the ROC curves of the four datasets using several detection thresholds in which TP rate is plotted on the Y axis and FP rate is plotted on the X axis. The best results (that maximizes sensitivity and specificity) are achieved using a threshold of 0.1163. At this cut-offs, the sensitivity is 100% and specificity is 92.85%. The ROC curves in Fig. 9 indicate that the proposed model performs better at identifying gaseous emboli than at identifying solid emboli for the concentrations C = 0.025 µl/ml and C = 0.05 µl/ml at high MI (0.6), the ROC curves produce an AUC of 97.44 and 96.93% respectively. On the contrary, for the concentration C = 0.025 µl/ml at low MI (0.2), the classifier recognizes better solid emboli than gaseous emboli. The classification performances for gaseous and solid emboli are quite similar for the concentration C = 0.05 µl/ml at low MI (0.2).

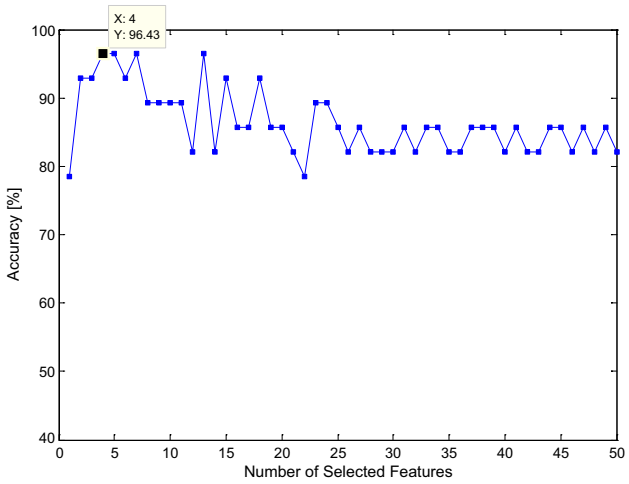

Fig. 8 Classification rates vs number of selected features with concentration of microbubbles (0.025 µl/ml) at high MI (0.6)

Table 5 illustrates the analysis of ROC curves using DEFS algorithm. The best value of accuracy based on the optimal threshold is obtained for concentration C = 0.025 µl/ml at high MI (0.6), the ROC point at (0.07, 1) produces its highest accuracy (96.42%), with an AUC of 97.44%. For all the acquisitions a significant improvement in terms of accuracy, sensitivity, and specificity is observed when using feature selection based on DEFS algorithm.

Table 6 illustrates the confusion matrix of the proposed system. The numbers of correct and incorrect predictions made by the proposed model compared to the target values in the test data are shown in Table 6. For example, at microbubble concentration 0.025 µl/ml and high MI (0.6) the proposed classification model succeeded in classifying 14 gaseous embolus out of 14 (Sensitivity = 100%) and 13 solid embolus out of 14 (Specificity = 92.85%). Thus 1 solid embolus is not recognized i.e. classified as gaseous embolus, the gaseous embolus are all recognized.

In order to validate the proposed approach; we compared the obtained results in this study with those obtained in a recently published study [13] on the same backscatter RF signals (refer to Fig. 10). The average percentage of correct classification of microemboli using DEFS algorithm with SVM classifier for two microbubbles concentrations (0.025 µl/ml and 0.05 µl/ml) at high and low mechanical index (0.2 and 0.6) are given in Table 7.

Table 5 Generalisation performances using feature selection based DEFS algorithm

	$C = 0.025$ µl/ml				$C = 0.05$ µl/ml			
	Low MI (0.2)		High MI (0.6)		Low MI (0.2)		High MI (0.6)	
	DEFS	Nbr of selected features	DEFS	Nbr of selected features	DEFS	Nbr of selected features	DEFS	Nbr of selected features
Sensitivity (gaseous emboli)	85.71%	07	100%	04	92.85%	05	100%	07
Specificity (solid emboli)	100%		92.85%		92.85%		85.71%	
Accuracy	92.85%		**96.42%**		92.85%		92.85%	
AUC (area under curve)	96.93%		**97.44%**		96.93%		96.93%	
OT: optimal threshold	0.4190		0.1163		0.0326		0.0898	

The threshold of 0.1163 provides the best AUC and its corresponding accuracy represented in bold

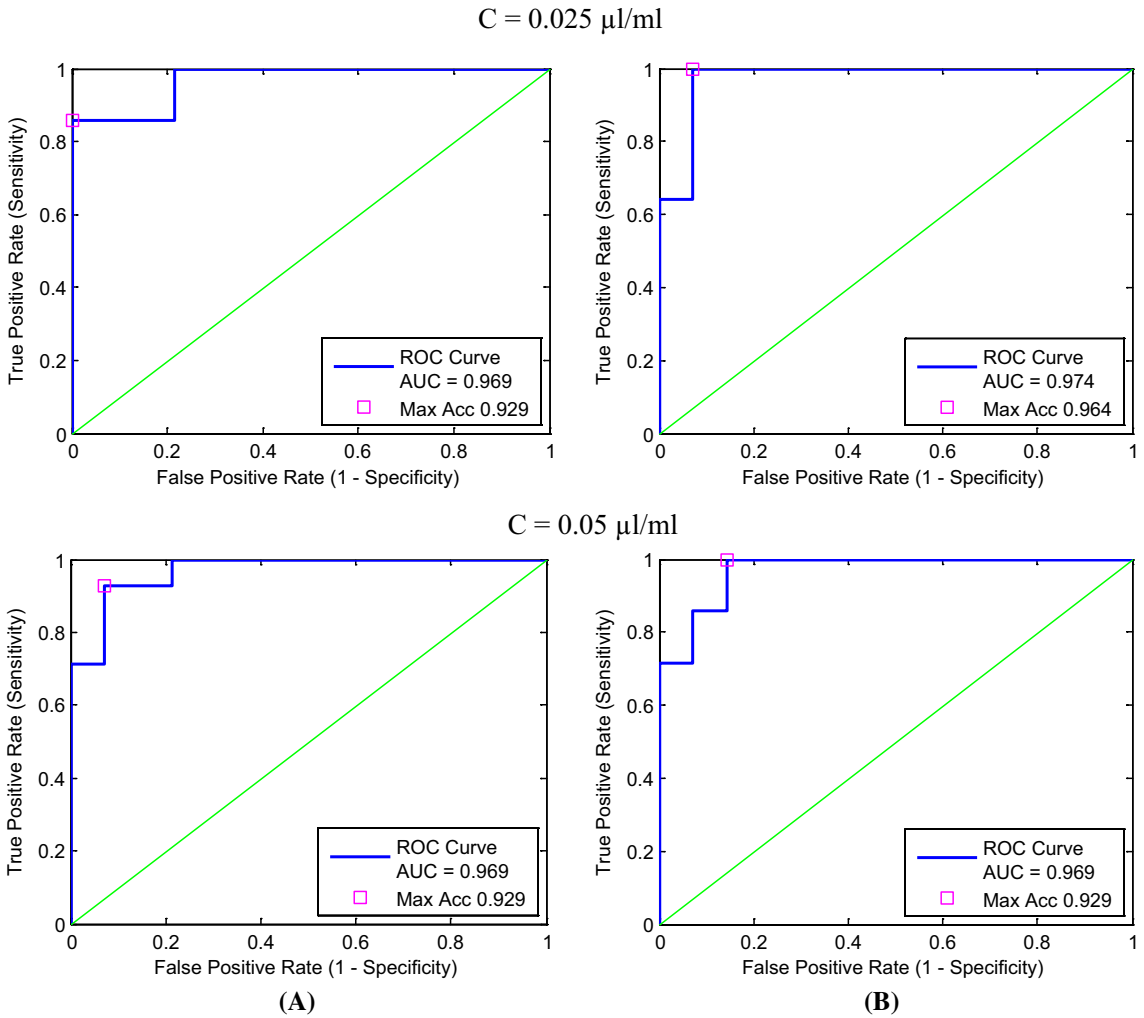

Fig. 9 ROC curve at different detection thresholds: **a** MI = 0.2, **b** MI = 0.6 for two microbubbles concentrations

Table 6 Confusion matrix of the proposed model

C = 0.025 µl/ml							
		Predicted					
		Acquisition 1. Low MI (0.2)		Nbr of selected features	Acquisition 2. High MI (0.6)		Nbr of selected features
		Gaseous emboli	Solid emboli		Gaseous emboli	Solid emboli	
Actual class	Gaseous emboli	12	2	7	14	0	4
	Solid emboli	0	14		1	13	
C = 0.05 µl/ml							
		Acquisition 3. Low MI (0.2)		Nbr of selected features	Acquisition 4. High MI (0.6)		Nbr of selected features
		Gaseous emboli	Solid emboli		Gaseous emboli	Solid emboli	
Actual class	Gaseous emboli	13	1	5	14	0	7
	Solid emboli	1	13		2	12	

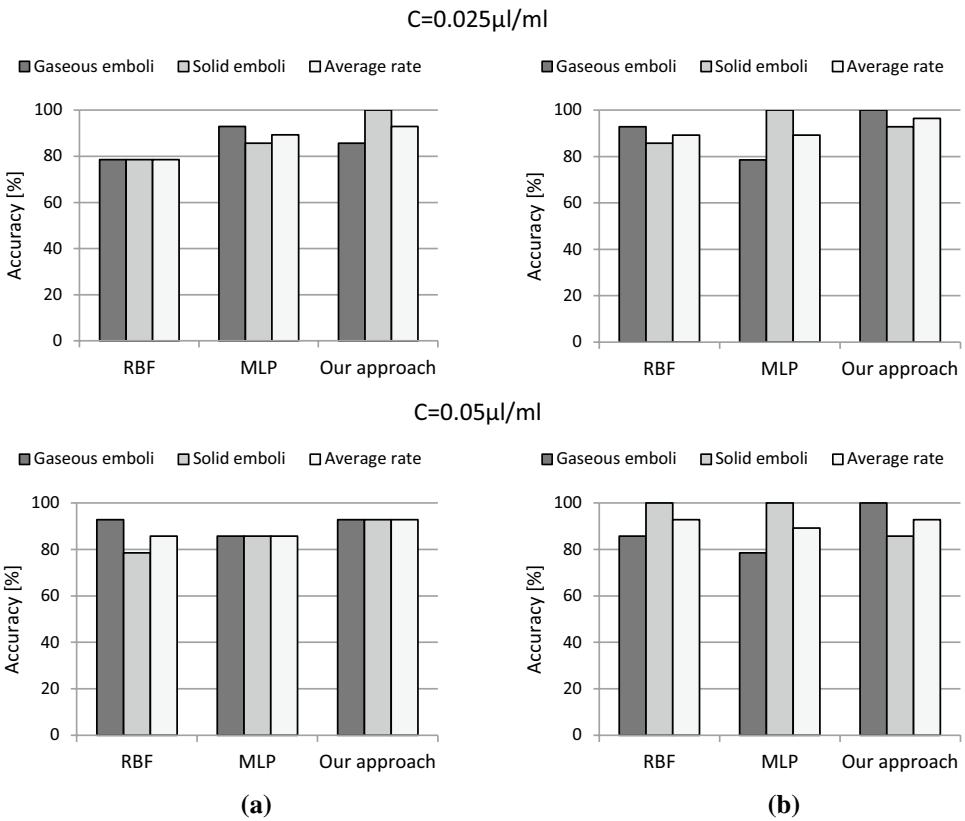

Fig. 10 Generalisation performances using DEFS algorithm and comparison with the results obtained in Ref. [13]: **a** MI = 0.2, **b** MI = 0.6 for two microbubbles concentrations

Discussion

In this experimental study we exploit RF signals in the detection and the classification of microemboli into gaseous or solid embolus. Several features are evaluated from the detail coefficients using DWT technique. It should be noted that the features used in this study are the same used in the work by Aydin et al. [7]. These features are used as inputs to the classification models without feature selection method. The average classification rate doesn't exceed 89.28% for all datasets, this can be explained by the fact that even the more powerful among the existing machine

Table 7 Generalisation performances using DEFS algorithm and comparison with the results obtained in Ref. [13]

	Methods [accuracy (%)]											
	C = 0.025 µl/ml						C = 0.05 µl/ml					
	Low MI (0.2)			High MI (0.6)			Low MI (0.2)			High MI (0.6)		
	Ref. [13]		Our approach	Ref. [13]		Our approach	Ref. [13]		Our approach	Ref. [13]		Our approach
	RBF	MLP		RBF	MLP		RBF	MLP		RBF	MLP	
Gaseous emboli	78.57	92.85	85.71	92.85	78.57	100	92.85	85.71	92.85	85.71	78.57	100
Solid emboli	78.57	85.71	100	85.71	100	92.85	78.57	85.71	92.85	100	100	85.71
Average rate	78.57	89.28	**92.85**	89.28	89.28	**96.42**	85.71	85.71	**92.85**	92.85	89.28	**92.85**

learning algorithms tend to get confused when supplied with a large number of features.

Building quantitative models (classifiers) using a large number of features most often requires using a smaller set a features than the initial one. Indeed, a too large number of features feed to a model (classifier) results in a too large number of parameters, leading to overfitting and poor generalization abilities [27]. It is noteworthy, in our case, the original data set contains d features ($d=50$), an extensive search of all possible combinations would involve the design of 2^{d-1} different models. This value grows exponentially, making an exhaustive search impractical even for moderate values of d. In order to reduce the dimensionality and select a relevant set of features, we implemented a wrapper feature selection approach based on differential evolution algorithm. For all the acquisitions a significant improvement in the classification rates is observed when using feature selection based on DEFS algorithm. The average classification rate goes down when the number of selected features gets larger which validates that learning might be deteriorated by irrelevant features (refer to Fig. 8).

In order validate the proposed approach; we compared the obtained results in this study with those obtained in a recently published study [13] on the same backscatter RF signals (refer to Table 7). In Ref. [13] the authors employed a neural network (MLP and RBF) analysis using the fundamental and the second harmonic components information contained in the RF signal backscattered by an embolus. The experimental results show clearly that our proposed method achieves better average classification rates compared to the method cited in [13] using also the same backscatter RF signals.

The superiority of SVM over the Neural Network approach can be explained by the fact that SVM has a high capacity for generalization using limited numbers of training data points; furthermore, SVMs don't have local extrema problems that are present for traditional neural networks, which involve large numbers of training patterns. The performance of SVMs relies on the choice of kernel type and kernel parameters, but this dependence is less influential.

It is noteworthy that the results depicted by Tables 3, 4, 5, 6 and 7 are reproducible. The best results appear in bold. The algorithm has only access to the training and validation sets, the test set is kept unseen in the selection process of the best model. The test set is used only for the assessment of the model selected by the cross-validation technique.

According to the obtained results, one may need to combine other types of approaches (e.g., filter and embedded) in order to improve the discriminative power of the proposed method. The processing time is an essential consideration if we have to implement this approach in clinical decisions. It should be noted that the training/feature selection phase lasts for a few minutes while the processing time for the test phase (classification) is less than 1 s. The implementation of such algorithm in real time applications makes also the investigation of the feasibility of emboli signals detection systems using RF signals worthwhile.

Conclusion

Emboli detection and classification remain promising research due to the correlation between embolism consequences and embolus nature (gaseous or solid emboli). The detection and classification of circulating microemboli is nowadays considered as a main challenge in the field of emboli detection.

The results presented in this experimental study demonstrate the usefulness of RF ultrasound signal processing in detection and classification of microemboli. A first proof of the concept of emboli classification based on the combination of a time–frequency based feature extraction technique (discrete wavelet transform), feature selection (DEFS), and backscatter RF signals is demonstrated. The results indicated that feature selection not only has the ability to find the most relevant set of inputs that result in higher average classification rate but also has the ability to reduce the size of feature vector. We demonstrated in this experimental study that combining DEFS algorithm and discrete wavelet transform provides better average classification rates (96.42%) in comparison to a previous study using also the same backscatter RF signal [13] that was evaluated extensively in a comparable manner.

The technique as suggested in this study proves to be effective in improving classification. The implementation of such algorithm in real time applications makes also the investigation of the feasibility of emboli signals detection systems using RF signal worthwhile. However, further validations in in-vivo situations are required to demonstrate the additional benefit.

Acknowledgements The authors would like to acknowledge the support of PHC Tassili France-Algérie 2014 (14 MDU 909).

Compliance with ethical standards

Conflicts of interest The authors state that there are no conflicts of interest.

Ethical approval This article does not contain any studies with human or animal subjects.

References

1. Molloy J, Markus HS (1999) Asymptomatic embolization predicts stroke and TIA risk in patients with carotid artery stenosis. Stroke 30(7):1440–1443

2. Aaslid R, Markwalder TM, Nornes H (1982) Noninvasive transcranial Doppler ultrasound recording of flow velocity in basal cerebral arteries. J Neurosurg 57(6):769–774
3. Pugsley W, Klinger L, Paschalis C, Treasure T, Harrison M, Newman S (1994) The impact of microemboli during cardiopulmonary bypass on neuropsychological functioning. Stroke 25(7):1393–1399
4. Ackerstaff RG, Jansen C, Moll FL (1996) Carotid endarterectomy and intraoperative emboli detection. Echocardiography 13(5):543–550
5. Georgiadis D, Grosset DG, Kelman A, Faichney A, Lees KR (1994) Prevalence and characteristics of intracranial microemboli signals in patients with different types of prosthetic cardiac valves. Stroke 25(3):587–592
6. Markus H, Israel D, Brown MM, Loh A, Buckenham T, Clifton A (1993) Microscopic air embolism during cerebral angiography and strategies for its avoidance. Lancet 341(8848):784–787
7. Aydin N, Marvasti F, Markus HS (2004) Embolic Doppler ultrasound signal detection using discrete wavelet transform. IEEE Trans Inf Technol Biomed 8(2):182–190
8. Aydin N, Padayachee S, Markus HS (1999) The use of the wavelet transform to describe embolic signals. Ultrasound Med Biol 25(6):953–958
9. Krongold BS, Sayeed AM, Moehring M, Ritcey J, Spencer MP, Jones DL (1999) Time-scale detection of microemboli in flowing blood with Doppler ultrasound. IEEE Trans Biomed Eng 46(9):1081–1089
10. Girault JM, Kouamé D, Ouahabi A, Patat F (2000) Micro-emboli detection: an ultrasound Doppler signal processing viewpoint. IEEE Trans Biomed Eng 47(11):1431–1439
11. Smith JL, Evans DH, Bell PR, Naylor AR (1998) A comparison of four methods for distinguishing Doppler signals from gaseous and particulate emboli. Stroke 29(6):1133–1138
12. Darbellay GA, Duff R, Vesin JM, Despland PA, Droste DW, Molina C et al (2004) Solid or gaseous circulating brain emboli: are they separable by transcranial ultrasound? J Cereb Blood Flow Metab 24(8):860–868
13. Benoudjit N, Ferroudji K, Bahaz M, Bouakaz A (2011) In vitro microemboli classification using neural network models and RF signals. Ultrasonics 51(3):247–252
14. Ferroudji K, Benoudjit N, Bahaz M, Bouakaz A (2011) Feature selection based on RF signals and KNN Rule: Application to microemboli classification. In: 2011 7th international workshop on systems, signal processing and their applications (WOSSPA) (pp 251–254). IEEE
15. Russell D, Brucher R (2002) Online automatic discrimination between solid and gaseous cerebral microemboli with the first multifrequency transcranial Doppler. Stroke, 33(8):1975–1980
16. Cowe J, Gittins J, Naylor AR, Evans DH (2005) RF signals provide additional information on embolic events recorded during TCD monitoring. Ultrasound Med Biol 31(5):613–623
17. Bolón-Canedo V, Sánchez-Maroño N, Alonso-Betanzos A, Benítez JM, Herrera F (2014) A review of microarray datasets and applied feature selection methods. Inf Sci 282:111–135
18. Khushaba RN, Al-Ani A, Al-Jumaily A (2009) Feature subset selection using differential evolution. In: Advances in neuro-information processing. Springer, Berlin Heidelberg, pp 103–110
19. Khushaba RN, Al-Ani A, Al-Jumaily A (2011) Feature subset selection using differential evolution and a statistical repair mechanism. Expert Syst Appl 38(9):11515–11526
20. Tadjudin S, Landgrebe DA (1999) Covariance estimation with limited training samples. IEEE Trans Geosci Remote Sens 37(4):2113–2118
21. Bishop CM (2006) Pattern recognition and machine learning, vol 128. Springer, New York, pp 225–338
22. Pal M, Mather PM (2005) Support vector machines for classification in remote sensing. Int J Remote Sens 26(5):1007–1011
23. Melgani F, Bruzzone L (2004) Classification of hyperspectral remote sensing images with support vector machines. IEEE Trans Geosci Remote Sens 42(8):1778–1790
24. Breiman L, Spector P (1992) Submodel selection and evaluation in regression. The X-random case. Int Stat Rev/revue internationale de Statistique 60:291–319
25. Strang G, Nguyen T (1996) Wavelets and filter banks. SIAM
26. Misiti M, Misiti Y, Oppenheim G, Poggi JM (1997) Wavelet toolbox. Matlab User's Guide
27. Ferroudji K, Benoudjit N, Bahaz M, Bouakaz A (2012) Selection of a suitable mother wavelet for microemboli classification using SVM and RF signals. In: 2012 24th international conference on microelectronics (ICM) (pp 1–4). IEEE
28. Rossi F, Lendasse A, François D, Wertz V, Verleysen M (2006) Mutual information for the selection of relevant variables in spectrometric nonlinear modelling. Chemom Intell Lab Syst 80(2):215–226
29. Donoho DL (1995) De-noising by soft-thresholding. IEEE Trans Inf Theory 41(3):613–627
30. Boashash B (1992) Estimating and interpreting the instantaneous frequency of a signal. II. Algorithms and applications. Proc IEEE 80(4):540–568
31. Cortes C, Vapnik V (1995) Support-vector networks. Mach learn 20(3):273–297
32. Tavakolan M, Yong X, Zhang X, Menon C (2016) Classification scheme for arm motor imagery. J Med Biol Eng 36(1):12–21
33. Wang L (2005) Support vector machines: theory and applications, vol. 177. Springer, New York
34. Hsu CW, Lin CJ (2002) A comparison of methods for multiclass support vector machines. IEEE Trans Neural Netw 13(2):415–425
35. Storn R (2008) Differential evolution research–trends and open questions. In: Advances in differential evolution. Springer, Berlin Heidelberg, pp 1–31
36. Palanchon P, Bouakaz A, Klein J, De Jong N (2005) Multifrequency transducer for microemboli classification and sizing. IEEE Trans Biomed Eng 52(12):2087–2092
37. SonoVue ® microbubbles. Bracco Research, Geneva
38. Piron J, Escoffre JM, Kaddur K, Novell A, Bouakaz A (2010) Enhanced gene transfection using ultrasound and Vevo Micromarker® microbubbles: microbubbles-assisted ultrasound and gene delivery. In: 2010 IEEE ultrasonics symposium (IUS) (pp 1586–1589). IEEE